CHAPTER TWO

MOBILE FADING CHANNELS

2.1 CHAPTER OVERVIEW

THE first part of this chapter considers the characterisation of mobile communication channels, outlining the different mechanisms contributing to the detrimental effects induced by such channels. A concise overview of the root and nature of AWGN is followed by a thorough study of multipath fading channels, covering aspects such as multipath propagation and Doppler spread. Frequency and time domain characterisation of multipath fading channels are discussed, including multipath channel characterisation parameters, such as excess delay and power delay profiles. The part on mobile radio channel characterisation is concluded with an investigation into Rayleigh and Rician faded signals. It should be noted that *log-normal shadowing* and large-scale fading effects, such as *path-loss* are not addressed in this study. The interested reader is referred to [37] for more detail on the latter, and to [35] for an explanation of log-normal shadowing.

The simulation or reproduction of the statistical behaviour of mobile communication channels is among the most significant phases in the design, analysis and evaluation of wireless communication systems. As such, several statistical models that explain the nature of such channels have been proposed in recent years. The second part of this chapter not only addresses the issue of accurate AWGN generation, but also presents novel complex channel simulator models for frequency selective (multipath) and non-selective Rayleigh and Rician fading channels, based on *Clarke*'s flat fading channel model [76]. Several implementation issues concerning these models, such as Doppler spread spectral shaping filter design and the implementation of Hilbert transformers are also investigated. The discussion on the simulation of mobile fading channels is concluded with a short discussion on the exponential decay modelling of typical power delay profiles.

2.2 ADDITIVE WHITE GAUSSIAN NOISE CHANNELS

An unavoidable limiting factor in the performance and capabilities of communication systems is AWGN. Understanding the origins and nature of AWGN is therefore crucial if effective counter measures, such as channel coding, are to be investigated or designed.

Degradation of communication system performance in noisy channel conditions can be attributed

to a variety of noise sources, including galactic noise (for example radiation), terrestrial noise, amplifier noise, interference from other communication systems, and last but not least, thermal noise caused by the motion of electrons in conducting media. The primary statistical characteristic of the resultant noise, created by adding the effects of all of the aforementioned noise sources, is a Gaussian amplitude distribution, described by the following PDF:

$$\rho(\eta(t)) = \frac{1}{\sigma_{\eta(t)}\sqrt{2\pi}} \exp\left(-\frac{\eta^2(t)}{2\sigma^2_{\eta(t)}}\right) \tag{2.1}$$

where $\sigma^2_{\eta(t)}$ is the noise variance or power. The principle spectral characteristic of AWGN is its essentially flat two-sided PSD for frequencies up to approximately 10^{12} Hz. Thus, AWGN possess equal power per Hertz for all frequencies currently of interest in mobile radio communication.

2.3 MULTIPATH FADING CHANNEL OVERVIEW

In a realistic mobile radio environment a single received signal is composed of a number of scattered waves, caused by the reflection and diffraction of the original transmitted signal by objects in the surrounding geographical area. These multipath waves combine at the receiver antenna to give a resultant signal which can vary widely in amplitude and phase [37, 42, 44]. Physical factors influencing the characteristics of the fading experienced by the transmitted signal are [42, 44]:

1. **Multipath propagation:** A constantly changing environment is created by the presence of reflecting objects and scatterers in the propagation channel, thereby altering the signal energy in amplitude, phase and time. The result of these effects is the arrival of multiple versions of the transmitted signal, each arriving signal differing from the other with respect to time and spatial orientation. Signal fading and/or distortion is the result of the fluctuations in signal strength, caused by the random phases and amplitudes of the different multipath components.

2. **Relative motion between the receiver and transmitter:** Relative motion between a transmitter and receiver results in frequency modulation (shift in carrier frequency) of each of the multipath components, due to the Doppler effect. The Doppler shift in carrier frequency can be negative or positive, depending on the relative direction of movement between the transmitter and receiver. For example, consider a transmitter moving at a velocity of $v_r(t)$ [m/s] relative to the receiver, transmitting on a carrier with a wavelength of λ [m]. The time-variant Doppler frequency shift, denoted by $f_{d,i}(t)$ [Hz], experienced by the i^{th} multipath *Line-of-Sight* (LOS) signal component entering the receiver antenna, is given by:

$$f_{d,i}(t) = \frac{v_r(t)}{\lambda} \cos\left(\theta_{A,i}(t)\right) \tag{2.2}$$

   where $\theta_{A,i}(t)$ is the angle of arrival of this received signal component. In this study only time varying Doppler frequencies are considered, since this is a common characteristic exhibited by typical mobile fading environments which current 2G and 3G, as well as future 4G communication systems are subjected to. The resultant effect of a time-varying Doppler shift is a phenomenon known as *Doppler spread* (see *Section* 2.4.3.3). Fixed Doppler frequencies are commonly encountered in narrowband *Very High Frequency* (VHF) communication systems, operating in flat fading channels.

3. **Motion of the reflecting objects and scatterers:** A time varying Doppler shift is induced on each multipath component if the reflecting objects and scatterers in the propagation channel are in motion. If the speeds of the reflecting objects and scatterers are small compared to the speed of the mobile, the effect this has on the fading of the multipath components can be ignored.

4. **Transmission bandwidth of the signal:** The bandwidth of a multipath channel can be quantified by the so-called *coherence bandwidth* (See section *Section* 2.4.3.2). If the bandwidth of a transmitted signal exceeds the coherence bandwidth of the channel it has to traverse, the signal suffers severe distortions in time, but not in amplitude. In such a case the signal experiences frequency selective fading. Conversely, if the coherence bandwidth exceeds the signal bandwidth, the signal experiences flat fading, i.e. severe amplitude distortion, but minimal time distortion.

2.4 MULTIPATH PROPAGATION

2.4.1 MULTIPATH CHANNEL IMPULSE RESPONSE

Multipath fading radio channels can be modelled as linear filters with time varying impulse responses [40–42, 44]. This filter-like nature of multipath fading channels' transfer functions is caused by the summation of the amplitudes and the delays between multiple arriving waves at a given time instance. Time dependence of such transfer functions is a result of relative motion between the transmitters and the receivers. Assuming the passband input signal to a multipath fading channel is $s(t)$, ignoring the effects of AWGN, the passband output signal of the channel is given by [40, 42]:

$$r(t) = s(t) \otimes h(t, \tau) \tag{2.3}$$

where $\otimes$ represents continuous-time convolution and $h(t, \tau)$ the time varying passband multipath fading channel impulse response. The variable t represents the time dependance in the variations of the channel impulse response due to motion, whereas τ represents the channel multipath delay for a fixed value of t. The passband channel impulse response can also be written as [40, 42]:

$$h(t, \tau) = \mathrm{Re}\left\{h_b(t, \tau) \exp\left[j2\pi f_c t\right]\right\} \tag{2.4}$$

where $h_b(t, \tau)$ is the baseband equivalent of the channel impulse response and f_c the carrier frequency of the passband input signal. Assuming the existence of L discrete multipath components in the multipath fading channel, this baseband channel impulse response can be written as [42]:

$$h_b(t, \tau) = \sum_{i=1}^{L} \beta_i(t, \tau)\delta\left(\tau - \tau_i\left(t\right)\right) \exp\left[j\left(2\pi f_c \tau_i(t) + \theta_i(t, \tau)\right)\right] \tag{2.5}$$

where $\beta_i(t, \tau)$ and $\tau_i\left(t\right)$ are the delay dependent instantaneous amplitude and time delay associated with the i^{th} multipath component, respectively. The instantaneous phase shift encountered by the i^{th} multipath component, due to its delay, is represented by $2\pi f_c \tau_i(t)$, whereas any other possible phase alterations experienced by this multipath component is incorporated in $\theta_i(t, \tau)$. To simplify *Eq.* (2.5), these phase delays are lumped together and represented by $\phi_i(t, \tau)$, where:

$$\phi_i(t, \tau) = 2\pi f_c \tau_i(t) + \theta_i(t, \tau) \tag{2.6}$$

If it is assumed that the time delay associated with each of the multipath components remains constant, the instantaneous baseband channel impulse response reduces to:

$$h_b(t, \tau) = \sum_{i=1}^{L} \beta_i(t)\delta\left(\tau - \tau_i\right) \exp\left[j\phi_i(t)\right] \tag{2.7}$$

where $\beta_i(t)$ and $\phi_i(t)$, respectively, are the time varying amplitude and phase alterations, experienced by the i^{th} multipath component, which has a fixed delay of τ_i.

Assuming that the channel is time invariant, or at least wide sense stationary over a small time or distance interval, the fixed delay baseband channel impulse response can be further simplified to [42]:

$$h_b(\tau) = \sum_{i=1}^{L} \overline{\beta}_i \delta(\tau - \tau_i) \exp\left[j\overline{\phi}_i\right] \tag{2.8}$$

where $\overline{\beta}_i$ and $\overline{\phi}_i$ are the time averaged values of $\beta_i(t)$ and $\phi_i(t)$, respectively. The normalised instantaneous amplitude variation, called the *instantaneous fading amplitude*, experienced by the i^{th} multipath component, is now given by:

$$\alpha_i(t) = \frac{\beta_i(t)}{\overline{\beta}_i} \tag{2.9}$$

2.4.2 POWER DELAY PROFILES

The power delay profile of a time variant multipath fading channel is given by: [37, 40, 42, 44]:

$$P(t,\tau) = |h_b(t,\tau)|^2 \tag{2.10}$$

By averaging *Eq.* (2.10) over time, the following time-invariant power delay profile is obtained [37, 42, 44]:

$$P(\tau) = \overline{|h_b(t,\tau)|^2} = \sum_{i=1}^{L} P(\tau_i)\,\delta(\tau - \tau_i) \tag{2.11}$$

where $P(\tau_i)$ is the average power in the i^{th} multipath component, given by [37, 42, 44]:

$$P(\tau_i) = \overline{\beta}_i^2 \tag{2.12}$$

In order to facilitate the simulation of digital communication systems in multipath fading environments, power delay profiles models that closely resemble real measured profiles are often used. Common models used include exponential decay profiles (see *Section* 2.6.3.3), Gaussian profiles, equal-amplitude two path (double spike) profiles and *Rummler*'s two ray model [44].

2.4.3 MULTIPATH CHANNEL PARAMETERS

The accurate comparison of different multipath fading channels are often difficult, if not impossible. Therefore parameters which grossly quantify such channels have been defined. These parameters can also be useful during the design of future wireless systems that will operate in multipath fading channel conditions.

2.4.3.1 TIME DISPERSION PARAMETERS

The delay time between signal transmission and reception of the first multipath component (denoted by the variable τ_1) is sometimes referred to as the *first arrival delay* [44]. Using this definition, the *excess delay* [37, 42, 44] of the i^{th} multipath component is the time difference between the first arrival delay and the delay time between signal transmission and reception of this multipath component.

The time dispersive properties of wideband multipath fading channels are commonly quantified by means of the following three parameters:

1. **Mean Excess Delay:** The mean excess delay gives an estimate of the average time delay experienced by a signal propagating through a multipath fading channel. It is obtained by calculating the

first moment of the power delay profile [37, 42, 44]:

$$\overline{\tau} = \frac{\sum_{i=1}^{L} P(\tau_i)\,(\tau_i - \tau_1)}{\sum_{i=1}^{L} P(\tau_i)} = \frac{\sum_{i=1}^{L} \overline{\beta}_i^2\,(\tau_i - \tau_1)}{\sum_{i=1}^{L} \overline{\beta}_i^2} \tag{2.13}$$

2. Root-Mean-Square Delay Spread: The *Root-Mean-Square* (RMS) delay spread is given by [37, 42, 44]:

$$\sigma_\tau = \sqrt{\overline{\tau^2} - (\overline{\tau})^2} \tag{2.14}$$

where:

$$\overline{\tau^2} = \frac{\sum_{i=1}^{L} P(\tau_i)\,(\tau_i - \tau_1)^2}{\sum_{i=1}^{L} P(\tau_i)} = \frac{\sum_{i=1}^{L} \overline{\beta}_i^2\,(\tau_i - \tau_1)^2}{\sum_{i=1}^{L} \overline{\beta}_i^2} \tag{2.15}$$

3. Maximum Excess Delay: The maximum excess delay (denoted by τ_{max}) [37, 42, 44] of a multipath fading channel is the excess delay of the last (L^{th}) multipath component. If a multipath channel is quantified only by its maximum excess delay, the last multipath component in the power delay profile is assumed to have an average power level of P_{drop} [dB] relative to the maximum average power level multipath component (a typical value for P_{drop} is -30 dB). Thus, the maximum excess delay is defined as [37, 42, 44]:

$$\tau_{max} = \tau_a - \tau_1 \tag{2.16}$$

where τ_a is the maximum delay at which a multipath component is within P_{drop} [dB] of the strongest arriving multipath component. It is important to note that the strongest component need not be the first arrival component, as it can be preceded by a number of non-minimum phase precursor multipath components.

2.4.3.2 COHERENCE BANDWIDTH

The coherence bandwidth [37, 42, 44] is a commonly used statistical measure of the range of frequencies over which a multipath fading channel's frequency response can be considered to be flat (see *Section* 2.5.1.1). In other words, the coherence bandwidth is the maximum frequency separation between two frequency components propagating through the channel, which exhibits a preset amplitude correlation. The coherence bandwidth is defined as [37, 42, 44]:

$$B_C = \frac{1}{\psi.\sigma_\tau} \tag{2.17}$$

where σ_τ is the RMS delay spread (see *Section* 2.4.3.1) and ψ a constant, dependent on the strength of the correlation between the two frequency components. Typical values for ψ are 50 and 5 for correlation values of approximately 0.9 and 0.5, respectively [42].

2.4.3.3 DOPPLER SPREAD AND COHERENCE TIME

The measure of spectral broadening (smearing), caused by the rate of change of multipath components, due to relative motion between the transmitter and the receiver, is known as Doppler spread [37, 42, 44]. The Doppler spread associated with the i^{th} received multipath component, $b_i(t)$, is defined as the single sided spectral width of the smearing experienced by a single tone carrier input

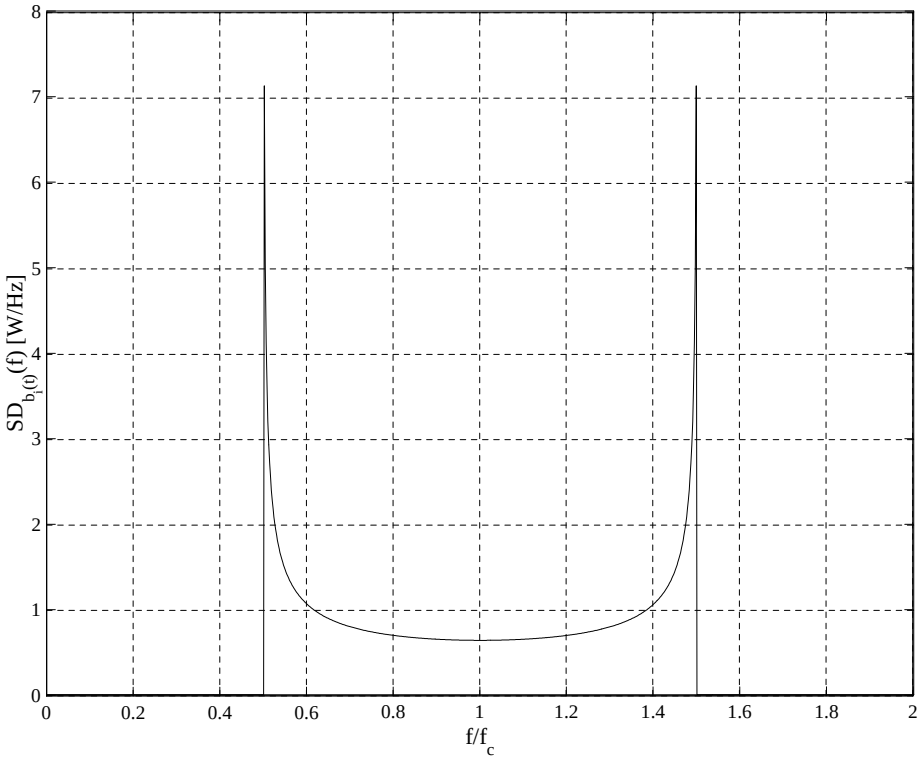

Figure 2.1: Classic Doppler Spectrum for $B_{D,i}/f_c = 0.5$ and $\sigma^2_{b_i(t)} = 1$

signal. Doppler spread is a function of the relative motion between the transmitter and receiver, as well as the angle of arrival of the scattered waves. For a sinusoidal channel input signal, experiencing a maximum Doppler shift of $\max\{f_{d,i}(t)\}$ (see *Eq.* (2.2)), it can be shown that the i^{th} multipath fading channel output signal's PSD approximates [37, 42, 44]:

$$SD_{b_i(t)}(f) = \begin{cases} \dfrac{\sigma^2_{b_i(t)}}{\pi\sqrt{\left(\max\{f_{d,i}(t)\}\right)^2-(f-f_c)^2}} & \text{if } |f-f_c| \leq \max\{f_{d,i}(t)\} \\ 0 & \text{if } |f-f_c| > \max\{f_{d,i}(t)\} \end{cases} \tag{2.18}$$

where f_c is the carrier frequency and $\sigma^2_{b_i(t)}$ is the average power of the transmitted signal. This PSD is usually referred to as a *classic Doppler spectrum* and is shown in *Fig.* 2.1 for $(\max\{f_{d,i}(t)\})/f_c = 0.5$ and $\sigma^2_{b_i(t)} = 1$. From *Eq.* (2.18) it is clear that the maximum Doppler spread is given by:

$$B_{D,i} = \max\{f_{d,i}(t)\} \tag{2.19}$$

The coherence time [42, 44] is a statistical measure of the time duration over which the flat fading channel impulse response is essentially time invariant. In other words, it is the maximum time interval between two received signals exhibiting a preset amplitude correlation. In general, it is given by [42, 44]:

$$T_{C,i} = \frac{\zeta}{B_{D,i}} \tag{2.20}$$

where ζ is a constant value dependent on the required amplitude correlation strength. Typical values for ζ are 1 and $9/(16\pi)$ for correlation values of 0.9 and 0.5, respectively [42].

2.5 SIGNAL FADING

2.5.1 TYPES OF SIGNAL FADING

The type of fading experienced by a signal propagating through a multipath fading channel is a function of both the nature of the transmitted signal and the characteristics of the channel. Different types of signals undergo different types of fading, depending on the signal parameters (bandwidth, etc.) and channel parameters (RMS delay spread, Doppler spread, etc.). Time and frequency dispersion mechanisms in multipath fading channels lead to four distinct types of signal fading, each of which is discussed in the following subsections.

2.5.1.1 MULTIPATH TIME DELAY SPREAD FADING EFFECTS

Signals propagating through a multipath fading channel undergo either frequency flat or frequency selective fading, due to time dispersion caused by multipath propagation [42]. These effects are discussed below:

1. **Flat Fading:** A signal propagating through a multipath fading channel that has a constant average gain and linear phase response over a larger bandwidth than the signal's bandwidth, experiences flat fading. The requirements for a signal to undergo flat fading are $B_{sig} << B_C$ and $T_{sig} >> \sigma_\tau$ [42], where B_{sig} and T_{sig} are the transmitted signal's bandwidth and reciprocal bandwidth, respectively. B_C and σ_τ are the channel's coherence bandwidth (see *Section* 2.4.3.2) and RMS delay spread (see *Section* 2.4.3.1), respectively.

   With this type of fading, the transmitted signal's spectral characteristics are preserved when it propagates through the channel. Only the received signal power fluctuates, due to the multipath effects. Since the reciprocal of the signal bandwidth is usually far greater than the RMS delay spread of the channel, modelling such channels as a single multipath component is a common approach [42].

2. **Frequency Selective Fading:** A signal propagating through a multipath fading channel that has a constant average gain and linear phase response over a smaller bandwidth than the signal's bandwidth, experiences frequency selective fading. This is due to the time dispersion experienced by the signals propagating through such a channel. The requirements for a signal to undergo frequency selective fading are $B_{sig} > B_C$ and $T_{sig} < \sigma_\tau$ [42], where B_{sig} and T_{sig} are the transmitted signal's bandwidth and reciprocal bandwidth, respectively. B_C and σ_τ are the channel's coherence bandwidth (see *Section* 2.4.3.2) and RMS delay spread (see *Section* 2.4.3.1), respectively.

   Under these conditions, the received channel output signal includes multiple versions of the transmitted signal, which are faded and delayed in time, resulting in ISI. Viewed in the frequency domain, certain frequency components of the received signal are faded differently from others.

2.5.1.2 DOPPLER SPREAD FADING EFFECTS

Signals propagating through a multipath fading channel undergo either fast or slow fading, due to the rate of change of the channel, caused by relative motion between the transmitter and the receiver. Signals propagating through the channel encounter either fast or slow fading effects [42], depending on the rate of change of the channel impulse response, as discussed below:

1. **Fast Fading:** If the channel impulse response changes rapidly within the symbol duration of the transmitted signal, the channel is called a *fast fading channel*. This implies that the coherence time (see *Section* 2.4.3.3) of the channel is smaller than the reciprocal bandwidth of the transmitted

signal. The requirements for a signal to undergo fast fading when propagating through a multipath fading channel are $T_{sig} > T_C$ and $B_{sig} < B_D$ [42], where B_{sig} and T_{sig} are the transmitted signal's bandwidth and reciprocal bandwidth, respectively. B_D and T_C are the channel's maximum Doppler spread and coherence time (see *Section* 2.4.3.3), respectively.

In the frequency domain, fast fading is characterised by frequency dispersion, due to Doppler spread. This frequency dispersion in turn causes time distortion on the transmitted signals.

2. **Slow Fading:** A *slow fading channel*'s impulse response varies at a rate much slower than the rate of change of the transmitted signal. Such a channel can be assumed to be static over a time period larger than the transmitted signal's reciprocal bandwidth interval. The requirements for a signal to undergo slow fading when propagating through a multipath fading channel are $T_{sig} << T_C$ and $B_{sig} >> B_D$ [42], where B_{sig} and T_{sig} are the transmitted signal's bandwidth and reciprocal bandwidth, respectively. B_D and T_C are the channel's maximum Doppler spread and coherence time (see *Section* 2.4.3.3), respectively.

2.5.2 FADING DISTRIBUTIONS

In the analysis of multipath fading channels, the phase and envelope distributions of the received multipath components of signals propagating through the channel are of great importance. Both the phase and envelope distributions are governed by the power of the unfaded or LOS signal component, relative to the faded or LOS signal component power in the total received multipath signal component. In the absence of a LOS signal component, the envelope distribution of a multipath component can be modelled as a Rayleigh PDF. Conversely, the presence of a LOS signal component dictates a signal envelope with a Rician PDF. The following subsections shed more light on the statistical nature of Rayleigh and Rician faded signals.

2.5.2.1 RAYLEIGH FADED SIGNALS

If the i^{th} received multipath component, denoted by $b_i(t)$, consists solely of a faded signal component, its enveloped, denoted by $\varepsilon_i(t)$, exhibits the Rayleigh distribution given by [37, 42, 44]:

$$\rho\left(\varepsilon_i(t)\right) = \begin{cases} \frac{\varepsilon_i(t)}{\sigma^2_{b_i(t)}} \exp\left(-\frac{\varepsilon_i^2(t)}{2\sigma^2_{b_i(t)}}\right) & \text{if } 0 \leq \varepsilon_i(t) < \infty \\ 0 & \text{if } \varepsilon_i(t) < 0 \end{cases} \tag{2.21}$$

where $\sigma_{b_i(t)}$ is the RMS value of $b_i(t)$ before enveloped detection. Since a Rayleigh distribution is obtained by setting $B_i = 0$ V in the expression for a Rician distribution (see *Eq.* (2.25) in *Section* 2.5.2.2), i.e. setting the LOS component in the signal $b_i(t)$ to zero, it follows that the curve shown in *Fig.* 2.2 for $K_i = -\infty$ dB depicts the Rayleigh PDF, described by *Eq.* (2.21). The mean value of the Rayleigh distribution is given by:

$$E\left[\varepsilon_i(t)\right] = \sigma_{b_i(t)} \cdot \sqrt{\frac{\pi}{2}} \tag{2.22}$$

where $E[\,\cdot\,]$ denotes expectancy. The variance (*Alternating Current* (AC) power in the envelope) of $\varepsilon_i(t)$ is given by:

$$\sigma_{\varepsilon_i^2(t)} = \sigma^2_{b_i(t)} \left(2 - \sqrt{\frac{\pi}{2}}\right) \tag{2.23}$$

Assuming a fixed phase channel input signal, it can be shown that the phase $\phi_i(t)$ of the i^{th} Rayleigh faded multipath signal component exhibits a uniform phase distribution, given by [37, 42, 44]:

$$\rho\left(\phi_i(t)\right) = \frac{1}{2\pi} \qquad \text{for } -\pi \leq \phi_i(t) \leq \pi \tag{2.24}$$

The curve for $K_i = -\infty$ dB in *Fig.* 2.3 depicts the phase distribution of a Rayleigh faded signal, as described by *Eq.* (2.24).

2.5.2.2 RICIAN FADED SIGNALS

When there are both LOS and *Non-Line-of-Sight* (NLOS) signal components, respectively denoted by $b_i^{LOS}(t)$ and $b_i^{NLOS}(t)$, present in the i^{th} received multipath component, the envelope of this multipath component, denoted by $\varepsilon_i(t)$, exhibits a Rician distribution, given by [42]:

$$\rho\left(\varepsilon_i(t)\right) = \begin{cases} \frac{\varepsilon_i(t)}{\sigma^2_{b_i^{NLOS}(t)}} \exp\left(-\frac{\varepsilon_i^2(t)+B_i^2}{2\sigma^2_{b_i^{NLOS}(t)}}\right) I_0\left(\frac{B_i.\varepsilon_i(t)}{\sigma^2_{b_i^{NLOS}(t)}}\right) & \text{if } B_i \geq 0 \text{ and } \varepsilon_i(t) \geq 0 \\ 0 & \text{if } \varepsilon_i(t) < 0 \end{cases} \tag{2.25}$$

where B_i is the maximum amplitude of $b_i^{LOS}(t)$, and $I_0\left(\cdot\right)$ is the modified Bessel function of the first kind and zero-th order. The parameters $\sigma^2_{b_i^{NLOS}(t)}$ and $\sigma^2_{b_i^{LOS}(t)}$ denote the time-average power in the NLOS and LOS signal components, respectively.

The nature of this distribution is governed by the power in the LOS signal component, relative to the power in the NLOS signal component. This ratio, usually given in [dB], is called the *Rician factor*. It is defined as follows:

$$K_i = 10\log_{10}\left(\frac{B_i^2}{2\sigma^2_{b_i^{NLOS}(t)}}\right) \tag{2.26}$$

As the LOS signal component's power tends to zero, and subsequently K_i tends to $-\infty$, the Rician PDF approaches a Rayleigh PDF. Considering the other extreme case where the LOS signal component becomes dominant, i.e. K_i tends to ∞, the Rician PDF approaches a Gaussian PDF. *Fig.* 2.2 shows Rician PDFs for $K_i = -\infty$ dB (Rayleigh), $K_i = 0$ dB (Rician) and $K_i = 6$ dB ($\approx$ Gaussian).

Assuming an input signal with a fixed phase θ_R, the phase distribution of a Rician faded multipath signal component is dependent on two factors: The NLOS signal component's phase distribution, given by *Eq.* (2.24), and the Rician factor (see *Eq.* (2.26)). For such a scenario, the PDF of the i^{th} Rician faded multipath component's phase $\phi_i(t)$, is given by [38, 77]:

$$\begin{aligned}\rho(\phi_i(t)) = &\frac{1}{2\pi}\exp\left(-\frac{B_i^2}{2\sigma^2_{b_i^{NLOS}(t)}}\right)\left\{1 + \frac{B_i}{\sigma_{b_i^{NLOS}(t)}}\sqrt{\frac{\pi}{2}}\cos\left(\phi_i(t)-\theta_R\right)\cdot\right. \\ &\left.\exp\left(\frac{B_i^2\cos^2\left(\phi_i(t)-\theta_R\right)}{2\sigma^2_{b_i^{NLOS}(t)}}\right)\left[1+\text{erf}\left(\frac{B_i\cos\left(\phi_i(t)-\theta_R\right)}{\sigma_{b_i^{NLOS}(t)}\sqrt{2}}\right)\right]\right\} \qquad \text{for } |\phi_i(t)| \leq \pi\end{aligned} \tag{2.27}$$

Fig. 2.3 shows the PDFs of the phases of Rician multipath signal components, calculated for the Rician factors $K_i = -\infty$ dB, $K_i = 0$ dB and $K_i = 6$ dB using *Eq.* (2.27).

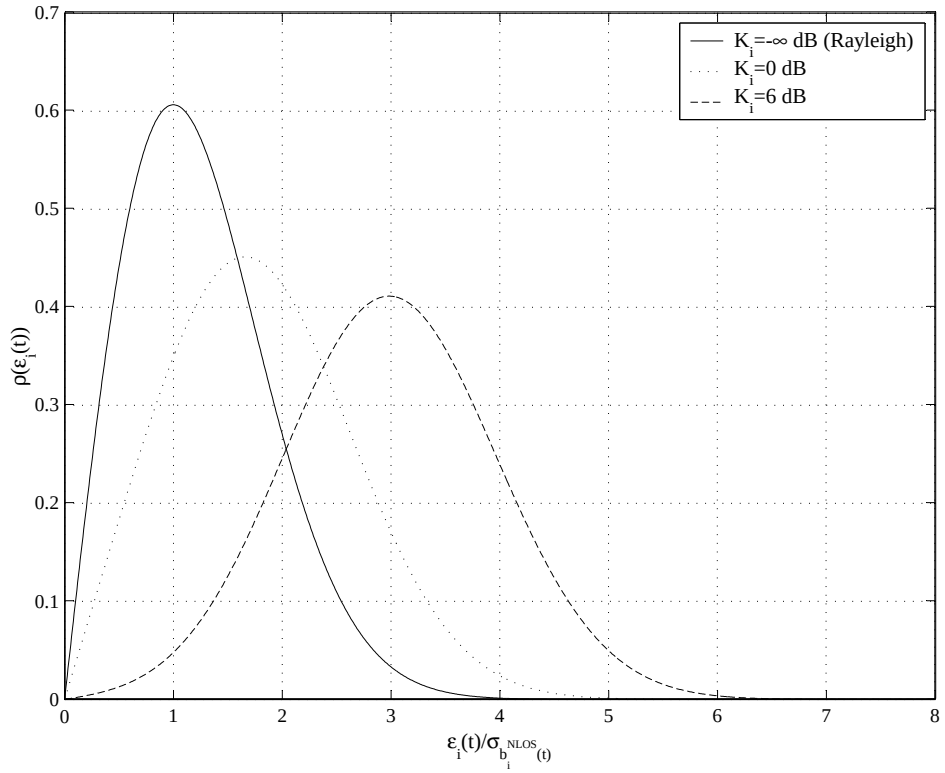

Figure 2.2: PDFs of the Envelopes of Rician Faded Multipath Signal Components for $K_i = -\infty$ dB (Rayleigh), $K_i = 0$ dB (Rician) and $K_i = 6$ dB ($\approx$ Gaussian)

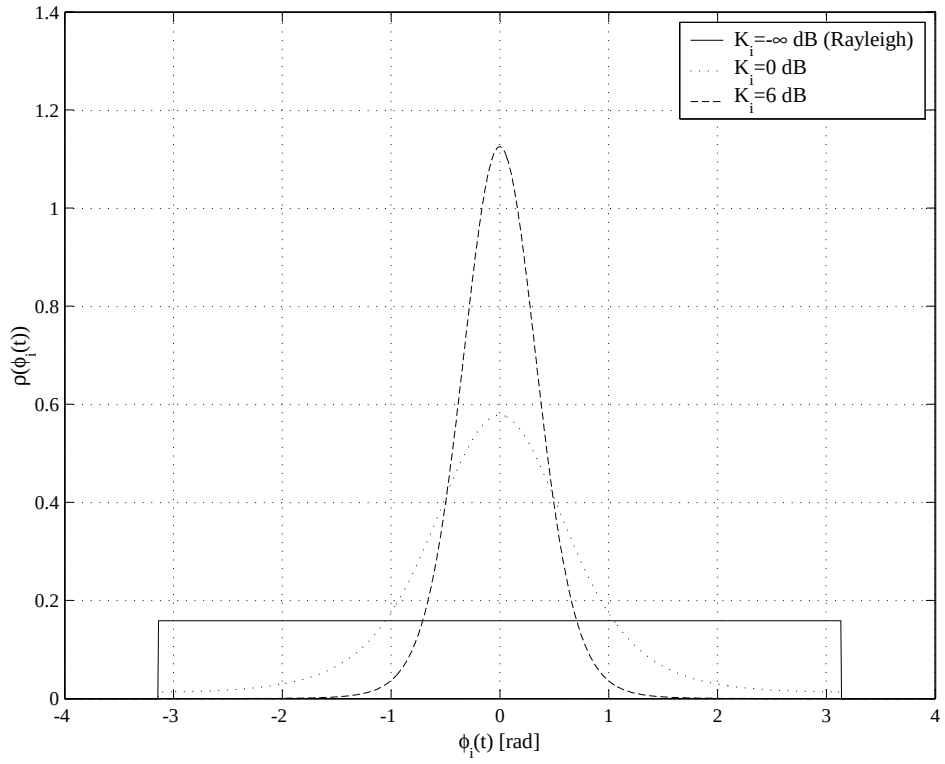

Figure 2.3: PDFs of the Phases of Rician Faded Multipath Signal Components for $K_i = -\infty$ dB, $K_i = 0$ dB and $K_i = 6$ dB with $\theta_R = 0$ rad

2.6 SIMULATING MOBILE RADIO CHANNELS

2.6.1 SIMULATING ADDITIVE WHITE GAUSSIAN NOISE CHANNELS

The next subsection gives a concise description of the accurate generation of AWGN. It is followed by a subsection that details the process whereby the variance of Gaussian noise samples can be scaled to obtain a specific E_b/N_0 value.

2.6.1.1 GENERATING GAUSSIAN DISTRIBUTED NOISE SAMPLES

When simulating mobile communication systems in AWGN channel conditions, transformation algorithms, such as the *Bray-Marsagalia* algorithm [78] and *Box-Muller* sine-cosine algorithm [79], are frequently utilised to generate samples that exhibit a Gaussian amplitude PDF with a zero mean and a variance of 1, using noise samples with uniformly distributed amplitude values ranging from 0 to 1 as inputs. Furthermore, the accurate simulation of AWGN channel conditions necessitates statistical independence between the uniformly distributed noise samples before being transformed to Gaussian distributed samples by the chosen transformation algorithm. Unfortunately, the uniform distribution random number generators implemented in programming languages such as C/C++, which are usually shift register-based PN generators, may not exhibit sufficient randomness. This is due to the fact that the sequence of samples that these generators produce for a given starting seed value, repeats too rapidly. In such cases it is good practise to rather use uniform distribution random number generator algorithms, such as the *Wichmann-Hill* algorithm [80]. Such random number generators exhibit lower statistical dependance between the uniformly distributed samples by increasing the sequence repetition length.

2.6.1.2 OBTAINING GAUSSIAN SAMPLES WITH THE REQUIRED NOISE VARIANCE AS DICTATED BY E_b/N_0

When investigating the performance of communication systems in typical mobile communication channel conditions, two quantities, namely the SNR and the E_b/N_0 [dB] value, are of importance. Although more commonly used in everyday jargon, the SNR, defined as the ratio of average transmitted signal power to noise power at the receiver output [81], is meaningless unless the noise equivalent bandwidth of the receiver is also specified. Consequently, the SNR is frequently normalised with respect to this bandwidth, resulting in the quantity E_b/N_0, which then becomes the independent variable in the performance measurements.

By stipulating the E_b/N_0 value for a specific performance measurement setup, it is possible to calculate the variance $\sigma^2_{\eta(t)}$ of the Gaussian noise samples required to realise the correct AWGN channel conditions. Assuming that the channel output signal enters the receiver through a noise limiting receive filter with the frequency response $H_{Rx}(f)$, the following relationship between the SNR and E_b/N_0 of coded binary communication systems holds:

$$SNR = \frac{\sigma^2_{s(t)}}{\sigma^2_{\eta(t)}} = \frac{E_b.f_{bit}}{N_0 \int_0^\infty |H_{Rx}(f)|^2 df} = \frac{E_c.(f_{bit}/R_c)}{N_0 \int_0^\infty |H_{Rx}(f)|^2 df} \tag{2.28}$$

where:
$\sigma^2_{s(t)}$ = Variance (power) of the transmitted signal.
$\sigma^2_{\eta(t)}$ = Variance (power) of the required Gaussian noise samples.
E_c = Energy in a transmitted coded bit.
R_c = Code rate.

E_b = Energy in an uncoded bit.
f_{bit} = Uncoded bit rate.
N_0 = Single-sided PSD level of AWGN.

Manipulating *Eq.* (2.28), an expression can be obtained for the required noise variance as a function of the specified E_b/N_0 [dB] ratio:

$$\sigma^2_{\eta(t)} = \frac{\sigma^2_{s(t)} \int_0^\infty |H_{Rx}(f)|^2 df}{10^{\left(\frac{1}{10}E_b/N_0\right)}.f_{bit}} \tag{2.29}$$

If Gaussian distributed noise samples are generated at a rate of f_{samp} [Hz] by a Gaussian transformation algorithm-based noise source, the effective noise bandwidth of the noise source is:

$$B_{ns} = \frac{f_{samp}}{2} \tag{2.30}$$

Furthermore, if the Gaussian PDF of the samples generated by the transformation algorithm has a variance of $\sigma^2_{ns(t)} = 1$, it follows that:

$$N_{ns}.B_{ns} = \sigma^2_{ns(t)} = 1 \tag{2.31}$$

where N_{ns} is the single-sided PSD level of the noise generated by the noise source. Using *Eq.* (2.30), it follows that this single-sided PSD level is given by:

$$N_{ns} = \frac{2}{f_{samp}} \tag{2.32}$$

Thus, the power of the noise generated by the transformation algorithm at the output of the receive filter is given by:

$$\sigma^2_{r(t)} = N_{ns} \int_0^\infty |H_{Rx}(f)|^2 df = \frac{2}{f_{samp}} \int_0^\infty |H_{Rx}(f)|^2 df \tag{2.33}$$

Since the required noise variance is given by *Eq.* (2.29), it follows that the factor k_η whereby the noise variance of the noise samples, generated by the transformation algorithm-based noise source, must be scaled, is given by:

$$k_\eta = \frac{\sigma^2_{\eta(t)}}{\sigma^2_{r(t)}} \tag{2.34}$$

Using *Eq.* (2.29), *Eq.* (2.33) and *Eq.* (2.34), the following expression for k_η is obtained:

$$k_\eta = \frac{\sigma^2_{s(t)}.f_{samp}}{10^{\left(\frac{1}{10}E_b/N_0\right)}.2.f_{bit}} \tag{2.35}$$

Since the scaling factor k_η is a power scaling factor, it follows that the noise samples generated by the transformation algorithm has to be scaled by $\sqrt{k_\eta}$ in order to produce Gaussian noise samples with a variance of $\sigma^2_{\eta(t)}$.

2.6.2 CLARKE'S FLAT FADING CHANNEL MODEL

Constructing an L-path statistical multipath fading channel simulator is accomplished by using L unique statistical flat fading channel simulators (see *Section* 2.6.3). Several statistical flat fading simulator models exist, among which the *Jakes* [82] and *Clarke* [76] models are the most popular.

This study makes use of the *Clarke* flat fading channel simulator model. Note that empirical multipath fading channel simulator models fall beyond the scope of this study.

2.6.2.1 BACKGROUND

Based on the statistical characteristics of the scattered electromagnetic fields constituting the signal entering a moving receiver, *Clarke* developed a model for flat fading channels [76]. The assumptions that he made in the development of this model are:

- The transmitter is fixed and employs an omnidirectional vertically polarised antenna.
- The field incident on the receiver consists of M_{apw} azimuthal plane waves.
- Each of the M_{apw} azimuthal plane waves have an arbitrary carrier phase. These phase angles are assumed to be uniformly distributed, as described by *Eq.* (2.24).
- Each of the M_{apw} azimuthal plane waves have an arbitrary angle of arrival.
- The M_{apw} azimuthal plane waves have equal average amplitudes, implying the absence of a LOS path.

Using *Rice*'s analysis [83, 84], which proved that an electromagnetic field can be expressed in an in-phase and quadrature form, *Clarke* showed [76] that the received signal's electromagnetic field is given by [42]:

$$E(t) = E_I(t)\cos(2\pi f_c t) - E_Q(t)\sin(2\pi f_c t) \tag{2.36}$$

with:

$$E_I(t) = E_o \sum_{j=1}^{M_{apw}} A_j(t)\cos(\phi_j(t)) \tag{2.37}$$

and:

$$E_Q(t) = E_o \sum_{j=1}^{M_{apw}} A_j(t)\sin(\phi_j(t)) \tag{2.38}$$

where E_o is the constant amplitude of the transmitted signal's electromagnetic field. The variables $A_j(t)$, and $\phi_j(t)$ are random variables representing the amplitude and phase of the j^{th} scattered electromagnetic field component arriving at the receiver, respectively. *Clarke* showed [76] that the variables $E_I(t)$ and $E_Q(t)$ are both Gaussian random processes. Therefore, the envelope of the received electromagnetic field, given by:

$$\varepsilon(t) = |E(t)| = \sqrt{(E_I(t))^2 + (E_Q(t))^2} \tag{2.39}$$

exhibits the Rayleigh distribution, given by *Eq.* (2.21).

2.6.2.2 CLASSIC IMPLEMENTATION OF CLARKE'S FLAT FADING CHANNEL MODEL

The classic flat fading channel simulator [39, 42, 44] for the i^{th} multipath component, based on *Clarke*'s model [76], is shown in *Fig.* 2.4. The simulator receives an input signal (denoted by $u_i(t)$) and creates in-phase (denoted by $u_i(t)$) and quadrature (denoted by $\hat{u}_i(t)$) versions of this signal using a *Hilbert transformer* (denoted by the block HT_i).

The quadrature signal $\hat{u}_i(t)$ is multiplied by $n_i^Q(t)$, which is a Doppler filtered version of zero-mean Gaussian noise, generated by noise generator $G_i^Q(t)$. The Doppler lowpass filter $DF_i^Q(f)$ is designed

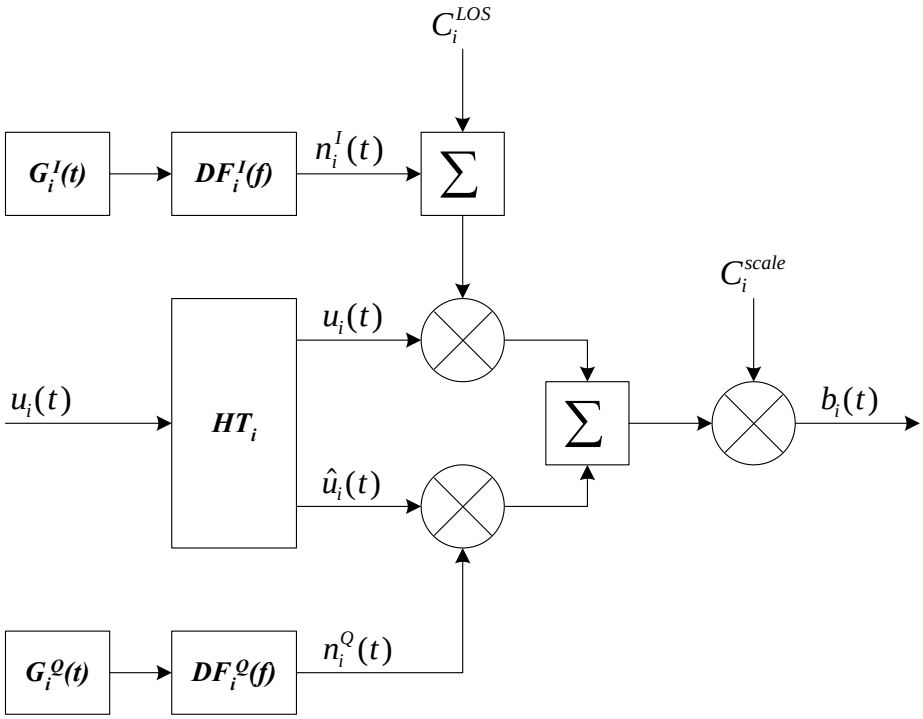

Figure 2.4: Classic Flat Fading Channel Simulator Based on *Clarke*'s Model

(see *Section* 2.6.2.4.2) to approximate a baseband equivalent of the output signal PSD shown in *Fig.* 2.1 [85]. The filter coefficients are also scaled to ensure that $n_i^Q(t)$ has unity power.

The in-phase signal $u_i(t)$ is multiplied by a linear combination of $n_i^I(t)$, which is a Doppler low-pass filtered version of the zero-mean Gaussian noise, generated by noise generator $G_i^I(t)$, and a constant value C_i^{LOS}, which facilitates a LOS signal component in the simulator output signal. The Doppler filter $DF_i^I(f)$ is identical to $DF_i^Q(f)$.

The output of the flat fading channel simulator, denoted by $b_i(t)$, is given by:

$$b_i(t) = C_i^{scale}\left[\left(n_i^I(t) + C_i^{LOS}\right)u_i(t) + n_i^Q(t).\hat{u}_i(t)\right] \tag{2.40}$$

where C_i^{scale} is a constant scale factor, which ensures that the power in the simulator input signal is equal to the power in the simulator output signal. The variable C_i^{scale} is calculated as follows: Assume the power in the input signal $u_i(t)$ is $P_{u_i(t)}$. Furthermore, let the power in the quadrature version of the input signal be $P_{\hat{u}_i(t)}$. The power in the output signal is now given by:

$$P_{b_i(t)} = \left(C_i^{scale}\right)^2\left[\left(1 + \left(C_i^{LOS}\right)^2\right)P_{u_i(t)} + P_{\hat{u}_i(t)}\right] \tag{2.41}$$

Since it is required that $P_{b_i(t)} = P_{u_i(t)} = P_{\hat{u}_i(t)}$, it can be shown that:

$$C_i^{scale} = \frac{1}{\sqrt{2 + \left(C_i^{LOS}\right)^2}} \tag{2.42}$$

As previously stated, the factor C_i^{LOS} is responsible for the presence a LOS signal component in the simulator output signal. The variable can be related to the Rician factor discussed in *Section* 2.5.2.2 as follows: Firstly, rewrite *Eq.* (2.40) so that the LOS and NLOS signal components, present in the simulator output, become clear:

$$b_i(t) = \underbrace{C_i^{scale}\left(n_i^I(t).u_i(t) + n_i^Q(t).\hat{u}_i(t)\right)}_{NLOS} + \underbrace{C_i^{scale}.C_i^{LOS}.u_i(t)}_{LOS} \tag{2.43}$$

It can be shown that the Rician factor, which is the ratio (in [dB]) of the average LOS signal component power to the average NLOS signal component power, simplifies to:

$$K_i = 20\log_{10}\left(\frac{C_i^{LOS}}{\sqrt{2}}\right) \tag{2.44}$$

2.6.2.3 COMPLEX IMPLEMENTATION OF CLARKE'S FLAT FADING CHANNEL MODEL

The use of the Hilbert transform in the classic *Clarke* flat fading channel simulator model of *Fig.* 2.4 can be eliminated by assuming that the i^{th} multipath signal component, transversing a multipath fading channel, has already been decomposed into real and imaginary parts, i.e.:

$$u_i(t) = \text{Re}\left\{u_i(t)\right\} + j.\,\text{Im}\left\{u_i(t)\right\} \tag{2.45}$$

Define a complex flat fading process, with an LOS component:

$$\varpi_i(t) = \alpha_i(t).\cos\left(\phi_i(t)\right) + C_i^{LOS} + j.\alpha_i(t).\sin\left(\phi_i(t)\right) \tag{2.46}$$

where $\alpha_i(t)$ and $\phi_i(t)$ are the instantaneous fading amplitude and phase of the i^{th} multipath signal component, respectively. It can easily be shown that the i^{th} complex multipath fading channel component is given by:

$$b_i(t) = \text{Re}\left\{b_i(t)\right\} + j.\,\text{Im}\left\{b_i(t)\right\} = \varpi_i(t).u_i(t) \tag{2.47}$$

Thus, the in-phase and quadrature outputs of the i^{th} flat fading channel, operating on a complex input signal, are given by:

$$\text{Re}\left\{b_i(t)\right\} = \text{Re}\left\{\varpi_i(t)\right\}.\text{Re}\left\{u_i(t)\right\} - \text{Im}\left\{\varpi_i(t)\right\}.\text{Im}\left\{u_i(t)\right\} \tag{2.48}$$

and:

$$\text{Im}\left\{b_i(t)\right\} = \text{Re}\left\{\varpi_i(t)\right\}.\text{Im}\left\{u_i(t)\right\} + \text{Im}\left\{\varpi_i(t)\right\}.\text{Re}\left\{u_i(t)\right\} \tag{2.49}$$

respectively. *Fig.* 2.5 shows a novel complex implementation of the *Clarke*'s flat fading channel that realises *Eq.* (2.48) and *Eq.* (2.49). From this figure it is clear that:

$$\text{Re}\left\{b_i(t)\right\} = C_i^{scale}\left[\left(n_i^I(t) + C_i^{LOS}\right).\text{Re}\left\{u_i(t)\right\} - n_i^Q(t).\text{Im}\left\{u_i(t)\right\}\right] \tag{2.50}$$

and:

$$\text{Im}\left\{b_i(t)\right\} = C_i^{scale}\left[\left(n_i^I(t) + C_i^{LOS}\right).\text{Im}\left\{u_i(t)\right\} + n_i^Q(t).\text{Re}\left\{u_i(t)\right\}\right] \tag{2.51}$$

Once again, the constant C_i^{scale} is chosen such that the channel simulator input signal power and output signal power have the same magnitude, resulting in an expression for C_i^{scale} which is identical to *Eq.* (2.42). Furthermore, following a similar approach as in *Section* 2.6.2.2, it can be shown that the Rician factor for the complex flat fading channel simulator is also given by *Eq.* (2.44).

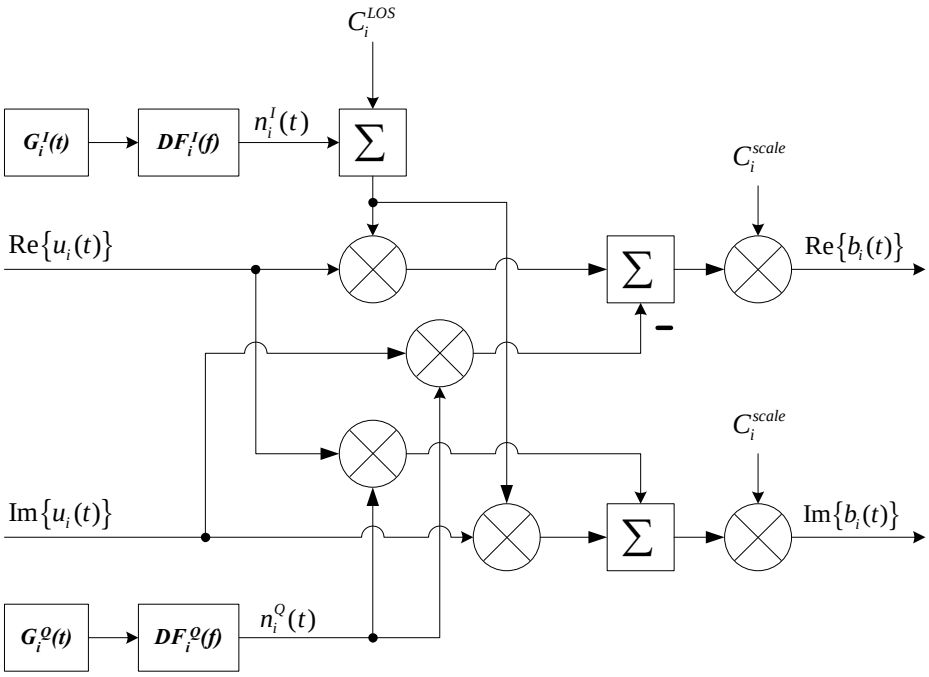

Figure 2.5: Complex Flat Fading Channel Simulator Based on *Clarke*'s Model

2.6.2.4 IMPLEMENTATION CONSIDERATIONS

2.6.2.4.1 Hilbert Transformer Realisation

Implementing the Hilbert transformer shown in *Fig.* 2.4 requires the use of a FIR filter and a delay line. The function of the FIR filter is to estimate the Hilbert transformation of the input signal in order to give the quadrature signal, whereas the delay line compensates for the FIR filter delay by the delaying the in-phase signal for a preset time period. The tap weights of a $(2F+1)$-tap Hilbert FIR filter are as follows [81]:

$$W(i) = \begin{cases} \frac{f_{samp}}{\pi . i} & \text{if } |i| \leq F, i \neq 0 \\ 0 & \text{if } i = 0 \text{ or } |i| > F \end{cases} \tag{2.52}$$

where f_{samp} is the sampling frequency used in the simulation. Note that the delay time induced by this FIR filter equals F sample periods.

2.6.2.4.2 Realisation of the Doppler Spread Spectral Shaping Filter

Assuming a maximum Doppler spread of $B_D = \max\{f_d(t)\}$ and a sampling period of T_{samp} [s], the Doppler filters used in the simulator of *Fig.* 2.4 can be approximated by using third order IIR filters with the following transfer function [38]:

$$DF(z) = C_{norm}\left[\frac{b_3 z^{-3} + b_2 z^{-2} + b_1 z^{-1} + b_0}{a_3 z^{-3} + a_2 z^{-2} + a_1 z^{-1} + a_0}\right] \tag{2.53}$$

where:

$$\begin{aligned}
b_0 &= b_3 = (2\pi B_D.T_{samp})^3 \\
b_1 &= b_2 = 3\,(2\pi B_D.T_{samp})^3 \\
a_0 &= 8 + 4A_{DF}.2\pi B_D.T_{samp} + 2B_{DF}\,(2\pi B_D.T_{samp})^2 + C_{DF}\,(2\pi B_D.T_{samp})^3 \\
a_1 &= -24 - 4A_{DF}.2\pi B_D.T_{samp} + 2B_{DF}\,(2\pi B_D.T_{samp})^2 + 3C_{DF}\,(2\pi B_D.T_{samp})^3 \\
a_2 &= 24 - 4A_{DF}.2\pi B_D.T_{samp} - 2B_{DF}\,(2\pi B_D.T_{samp})^2 + 3C_{DF}\,(2\pi B_D.T_{samp})^3 \\
a_3 &= -8 + 4A_{DF}.2\pi B_D.T_{samp} - 2B_{DF}\,(2\pi B_D.T_{samp})^2 + C_{DF}\,(2\pi B_D.T_{samp})^3
\end{aligned} \tag{2.54}$$

with:

$$\begin{aligned}
A_{DF} &= 1.55 \\
B_{DF} &= 1.090625 \\
C_{DF} &= 0.9953125
\end{aligned} \tag{2.55}$$

The variable C_{norm} is a constant scaling factor, dependent on the input signal's power, that ensures unity power in the filter output signal. *Fig.* 2.6 shows the frequency response of $DF(z)/C_{norm}$. Note that the frequency axis is normalised with respect to B_D.

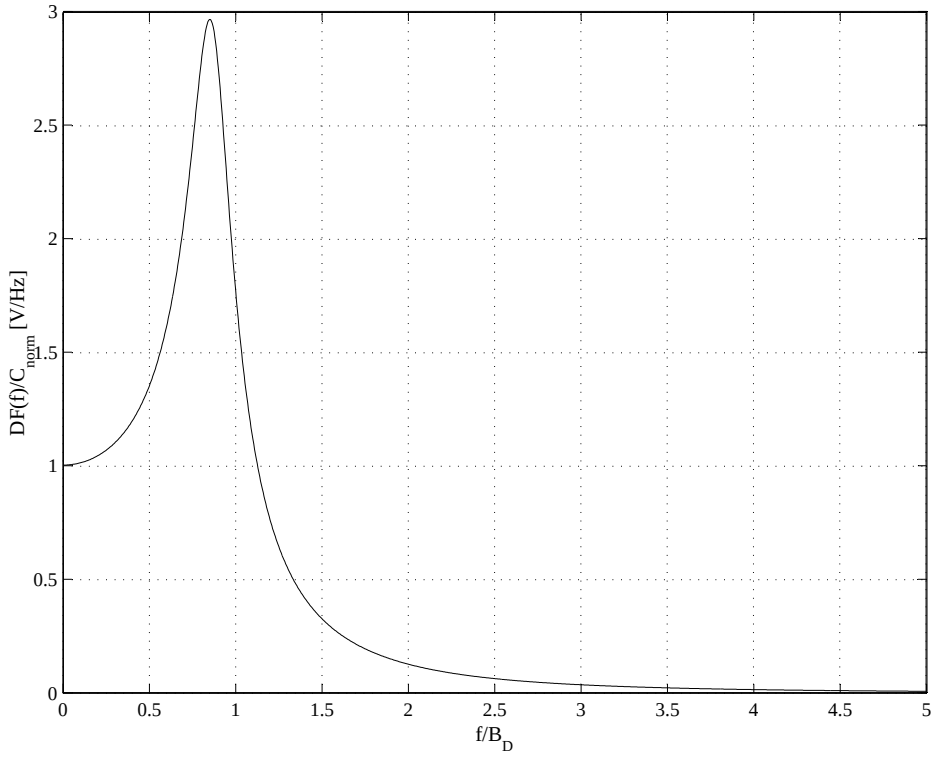

Figure 2.6: Frequency Response of the 3rd Order Doppler IIR Filter

Comparing the baseband frequency response of *Fig.* 2.6 with the required classic Doppler spectrum depicted in *Fig.* 2.1, it can be concluded that, due to the high spectral content in its tail end ($f > B_D$), the use of the proposed Doppler filter will result in more severe Doppler spread being produced by the simulator than by the mathematical model. Although higher order IIR Doppler filters will reduce this deviation from the mathematical model, the increased simulator complexity does not justify the improvement in the simulator's performance.

2.6.2.5 *OBTAINING CHANNEL STATE INFORMATION FROM THE CLARKE FLAT FADING CHANNEL SIMULATOR*

Perfect CSI, i.e. perfect fading amplitude and channel phase information, are easily obtainable from the *Flat Fading Channel Simulator*s (FFCS) shown in *Fig.* 2.4 and *Fig.* 2.5, respectively. The instantaneous fading amplitude of the i^{th} multipath component of a multipath fading channel employing such flat fading simulators, is calculated as follows:

$$\alpha_i(t) = \frac{\beta_i(t)}{\overline{\beta}_i} = \sqrt{\frac{\left(n_i^I(t) + C_i^{LOS}\right)^2 + n_i^Q(t)^2}{2 + \left(C_i^{LOS}\right)^2}} \tag{2.56}$$

where $\beta_i(t)$ and β_i are the instantaneous and average amplitude alterations experienced by the i^{th} multipath component, respectively. Calculation of the instantaneous phase change experienced by the i^{th} multipath component is accomplished as follows:

$$\phi_i(t) = -\arctan\left(\frac{n_i^Q(t)}{n_i^I(t) + C_i^{LOS}}\right) \tag{2.57}$$

Perfect, or near perfect knowledge of $\phi_i(t)$ is essential not only for coherent demodulation [86], but also for bit, frame and spreading sequence synchronisation. Estimation of the fading amplitude $\alpha_i(t)$ is required by channel coded systems employing CSI during decoder metric calculations. For example, the optimal operation of the iterative decoder structures associated with parallel, serial and hybrid concatenated codes [28, 30–33, 87], are dependent on accurate knowledge of $\alpha_i(t)$. Therefore, the use of CSI estimators in the receiver structures of modern communication systems, employing such concatenated codes, is indispensable. Refer to *Section* 3.3.5 for more information on practical CSI estimation techniques.

2.6.3 EMPLOYING CLARKE'S MODEL IN MULTIPATH FADING CHANNEL SIMULATORS

2.6.3.1 *CLASSIC MULTIPATH FADING CHANNEL SIMULATOR*

A frequency selective fading channel can be simulated using the general *Multipath Fading Channel Simulator* (MFCS) structure shown in *Fig.* 2.7 [39, 42, 44]. This simulator is capable of simulating a time-invariant multipath fading channel, consisting of L discrete and independently faded multipath components.

The simulator functions as follows: Firstly, an appropriate L-path power delay profile is chosen. L time-delayed versions of the transmitted signal are then created by using a L-tap delay line with delay times equal to that of the required power delay profile. Next, the time delayed signal $a_i(t)$, with $i = 1, 2, ..., L$, is scaled by the factor $\overline{\beta}_i$, which represents the average amplitude of the i^{th} multipath component, as specified by the power delay profile. These delayed and scaled signals are then processed by L unique FFCSs (denoted by blocks $Classic\,FFCS_1$ to $Classic\,FFCS_L$), such as the one shown in *Fig.* 2.4. Thus, it is possible to define a unique maximum Doppler frequency and Rician factor for each multipath component. The resultant outputs of the flat fading channel simulators, denoted by $b_i(t)$, with $i = 1, 2, 3, ..., L$, are then linearly combined to give the frequency selective fading channel's simulator output signal $r(t)$.

It is important to note that the power of the multi-path fading channel simulator's output signal $r(t)$ must equal the power of the transmitted signal $s(t)$. Since the L propagation paths undergo statisti-

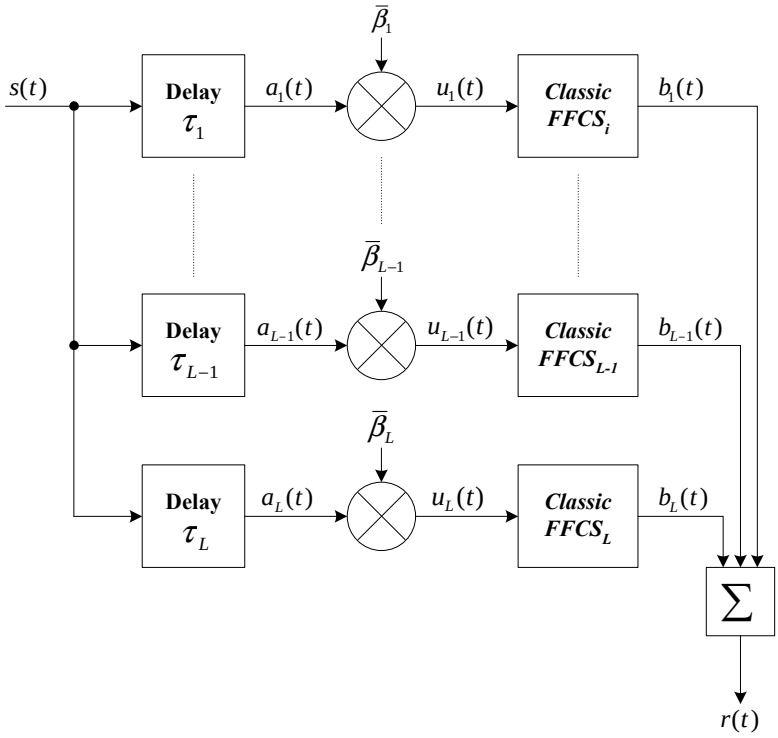

Figure 2.7: Classic Multipath Fading Channel Simulator

cally independent flat fading, it follows that the scaling factors $\overline{\beta}_i$, with $i = 1, 2, ..., L$, must conform to the following condition [86]:

$$\sum_{i=1}^{L} \left(\overline{\beta}_i\right)^2 = 1 \tag{2.58}$$

2.6.3.2 COMPLEX MULTIPATH FADING CHANNEL SIMULATOR

Fig. 2.8 shows an L-path complex multipath fading channel simulator, constructed using L distinct complex FFCSs (see *Section* 2.6.2.3), denoted by blocks $Complex\,FFCS_1$ to $Complex\,FFCS_L$. Aside from the fact that the complex multipath fading channel simulator processes complex input signals, it functions in a similar fashion as the classic implementation, described in *Section* 2.6.3.1. Furthermore, the average path gains $\overline{\beta}_i$, for $i = 1, 2, ..., L$, also need to comply with *Eq.* (2.58) in order to preserve equality between simulator input and output powers.

2.6.3.3 EXPONENTIAL DECAY MODELLING OF POWER DELAY PROFILES

Most measured outdoor power delay profiles appear to exhibit exponential decay profiles with superimposed spikes. As such, the use of exponential decay power delay profile models are used extensively when simulating the performance of digital communication systems in multipath fading channel conditions [42, 44]. An exponential decay power delay profile model is defined as follows:

$$P(\tau) = \frac{1}{P_{tot}} \exp\left(-\frac{\tau}{\tau_e}\right) \tag{2.59}$$

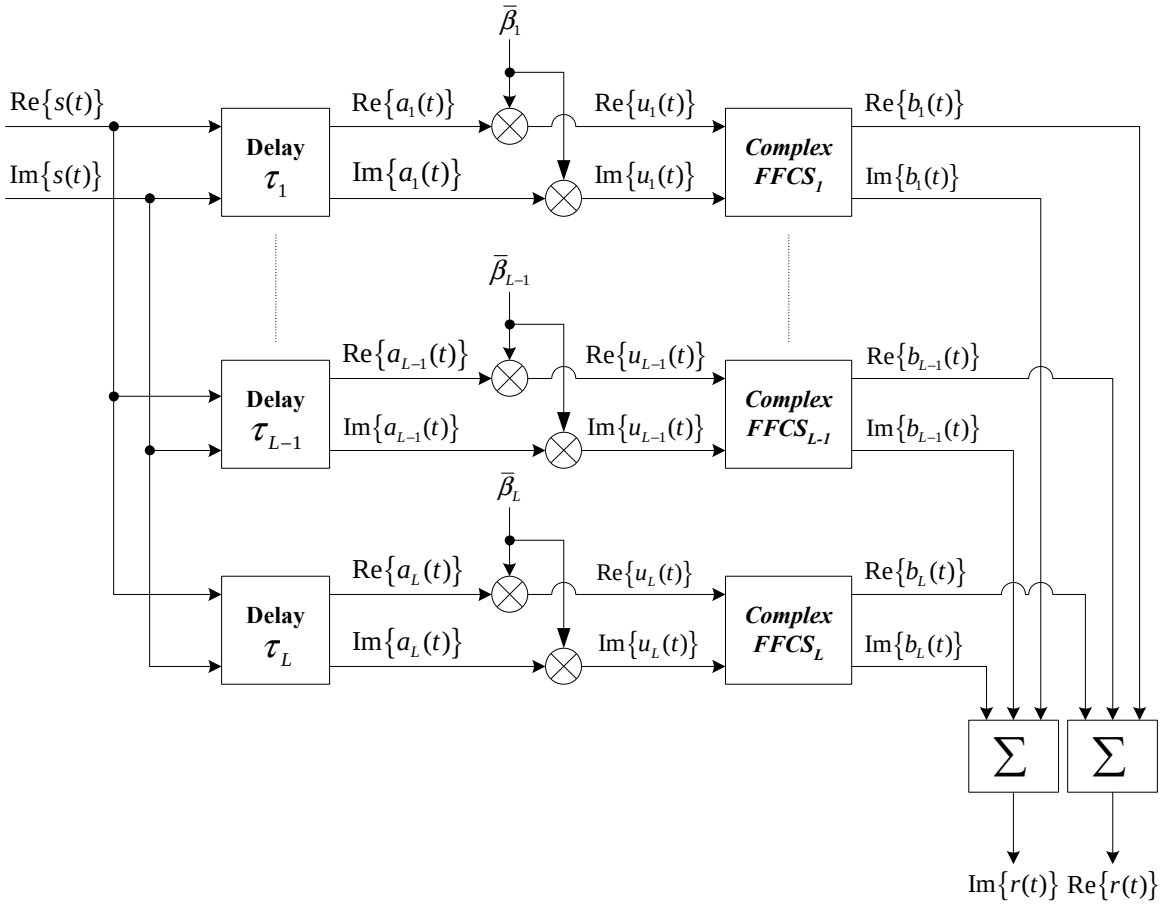

Figure 2.8: Complex Multipath Fading Channel Simulator

where P_{tot} is a normalisation factor and τ_e is the time constant of the profile. In order to comply with *Eq.* (2.58), the normalisation factor is calculated as follows:

$$P_{tot} = \sum_{i=1}^{L} P(\tau_i) = \sum_{i=1}^{L} \left(\overline{\beta}_i\right)^2 \tag{2.60}$$

Calculation of τ_e is dependent both on the maximum excess delay τ_{max} and the relative power drop between $P(\tau_{max})$ and $P(0)$, denoted by $P_{drop} = 10\log_{10}\left[P(\tau_{max})/P(0)\right]$ [dB]:

$$\tau_e = -\frac{\tau_{\max}}{\ln\left(10^{\frac{P_{drop}}{10}}\right)} \tag{2.61}$$

Recall from *Section* 2.4.3.1 that a typical value for P_{drop} is -30 dB.

2.7 CONCLUDING REMARKS

This chapter focused on the characterisation and statistical reproduction of realistic mobile communication channels, concentrating specifically on multipath fading channels. The chapter contains discussions on all aspects of AWGN, flat fading and frequency selective fading channel effects. Novel contributions made in this chapter are the following:

1. The erroneous Doppler spectral shaping IIR lowpass filter presented in [38] has been corrected. The improved filter is presented in *Section* 2.6.2.4.2.

2. A complex flat fading channel simulator model, extended from the classic *Clarke* model, is presented in *Section* 2.6.2.3. This model not only eliminates the use of Hilbert transformers, but also gives the communication engineer the capability to perform baseband flat fading channel simulations.

3. Extraction of CSI parameters from classic and complex flat fading channel simulators are addressed in *Section* 2.6.2.5.

4. An L-path complex multipath fading channel simulator, comprising of L unique complex flat fading channel simulators, is presented in *Section* 2.6.3.2. This model enables the communications engineer to conduct baseband frequency selective fading simulations.

5. A simple approach whereby realistic exponential decay power profiles can be created, is presented in *Section* 2.6.3.3.